Research Article | Vol. 31, No. 26 / 18 Dec 2023 / Optics Express 44622
Optics EXPRESS

Generic fabrication solution of freeform Fresnel optics using ultra-precision turning

YAOKE WANG,[1] JIANJIAN WANG,[2] AND PING GUO[1,*]

[1]Department of Mechanical Engineering, Northwestern University, Evanston, IL, USA
[2]Department of Mechanical Engineering, Tsinghua University, Beijing, China
[*]ping.guo@northwestern.edu

Abstract: Freeform Fresnel optics represent an emerging category of modern optics that reproduces powerful optical functionalities while maintaining an ultra-compact volume. The existing ultra-precision machining (UPM) technique faces technical challenges in meeting the fabrication requirements for freeform Fresnel optics because of the absence of appropriate geometry definition and corresponding tool path planning strategy to overcome the extreme asymmetry and discontinuity. This study proposes a new scheme for ultra-precision machining using four axes (X, Y, Z, C) to fabricate freeform Fresnel optics, including a general geometry description for freeform Fresnel optics, the quasi-spiral tool path generation strategy to overcome the lack of rotary symmetry, and the adaptive tool pose manipulation method for avoiding tool interference. In addition, the tool edge compensation and the adaptive timestep determination are also introduced to enhance the performance and efficiency of the proposed scheme. The machining of two exemplary freeform Fresnel lenses is successfully demonstrated. Overall, this study introduces a comprehensive routine for the fabrication of freeform Fresnel optics and proposes the adaptive tool pose manipulation scheme, which has the potential for broader applications in the ultra-precision machining of complex or discontinuous surfaces.

1. Introduction

Freeform Fresnel optics is an emerging category of modern optics that reproduces powerful optical functionalities of freeform optics while maintaining an ultra-compact volume that Fresnel optics provides. With an established design scheme [1], it enables advanced optical designs with an ultra-compact form. Freeform Fresnel optics designs have been proposed to realize compact wireless communications solution [2], LED illumination, and irradiance manipulation [3]. Furthermore, with the development of freeform Fresnel optics, optical systems composed of multiple optical components can be designed into a single element for compactness, low manufacturing cost, and unprecedented optical properties, such as those required in a VR/AR system [4]. Figure 1 shows the road map from freeform optics to freeform Fresnel lens designs for potential AR/VR applications. Freeform Fresnel optics combines the benefits of freeform optics that bring advanced optical performance and Fresnel lenses that provide an extremely compact form format. On the one hand, the Fresnel lens, as a representative miniaturized optical device, shows distinct advantages such as reduction in thickness, bulk volume, and cost of materials while maintaining equivalent performance to conventional optics [5]. On the other hand, Freeform optics, compared to spherical and aspherical lenses, have no rotationally symmetric axis in geometry, providing the potential of a highly tailored optical performance [6], including aberration correction [7], irradiance manipulation [8], and multiple foci [9]. They have emerged in a wide array of applications [10], including aerospace technology, biomedical engineering, optical communications, etc. Furthermore, freeform optics have been the enabling technology in the emerging head-up display, virtual reality, and augmented reality devices, showing an immeasurable market in the future.

#509238 https://doi.org/10.1364/OE.509238
Journal © 2023 Received 13 Oct 2023; revised 22 Nov 2023; accepted 24 Nov 2023; published 14 Dec 2023

Optics EXPRESS

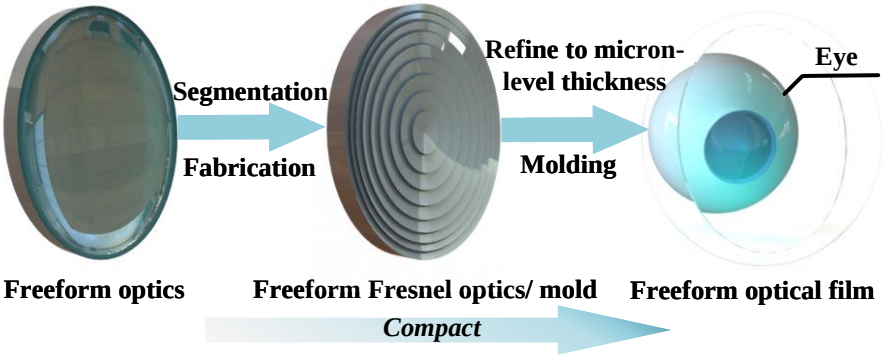

Fig. 1. Extremely compact optics potentially realized by freeform Fresnel optics.

The combination of freeform optics and Fresnel lens will bring both new optical performance with a compact form and open up new possibilities in the next-generation optics design. However, due to the lack of a scalable fabrication process feasible for the complexity of freeform Fresnel surfaces, existing theoretical designs have not been actually manufactured and demonstrated. Even though the theoretical design has been ahead for a while, the fabrication technology of freeform Fresnel optics remains uncultivated, preventing its wide application as highly expected. Among the existing processes for fabricating freeform or Fresnel optics, lithography-based techniques, including electron beam lithography [11], gray-scale lithography [12], and two-photon lithography [13], etc., are confined to the fabrication of micro-scale optics because of process efficiency. These cleanroom fabrication processes also require complex and costly post-processing to obtain an optical mold for mass production. Even though laser beam machining [14] is capable of machining optical features in variable scales across different materials, the optical performance is limited by resultant surface quality. The emerging nanoscale additive manufacturing [15] can be used to manufacture optical structures with extreme complexity, but it is still limited in process efficiency and only suitable for individual lens prototyping. Ultra-precision machining (UPM) has been the industrial standard for fabricating freeform optics, which has been extended to off-axis optics and lens arrays [16]. To further improve the feasibility of UPM on freeform optics fabrication, compensation methods [17], on-machine measurement [18], and fast-tool servo schemes [19] have been developed correspondingly. Besides, Fresnel optics in millimeter-scale is capable of being fabricated on both flat surfaces [20] and roller molds [21] using UPM. Also, customized multi-axis solutions have realized the fabrication of polygon Fresnel optics [22] and Fresnel lens arrays [23]. Even though UPM has demonstrated excellent feasibility in either freeform or Fresnel optics respectively, current UPM methods cannot be comprehensively applied to freeform Fresnel optics fabrication due to an unresolved critical technological gap – the existing UPM techniques cannot resolve the discontinuity and asymmetry of freeform Fresnel optics without undesired tool-workpiece interference. Here, a question comes naturally - whether there is a generic fabrication solution to cover freeform Fresnel optics or lens arrays defined by randomly given geometry instead of designing the fabrication process of variable optics individually. This is to say, the "generic fabrication solution" is supposed to solve the following technological gaps from four aspects in sequence:

(1) There is a lack of proper geometric definitions to generate machinable tool paths for freeform Fresnel optics. The existing geometric definitions of freeform Fresnel optics, even

Optics EXPRESS

the machinability of which is optimized by [24], could not translate to a machine tool path for UPM due to the existence of discontinuity. Therefore, a geometry definition method specifically designed for UPM is proposed in this study that converts a desired freeform surface into a machinable freeform Fresnel description.

(2) Due to the lack of rotary symmetry and discontinuity between facets in freeform Fresnel optics, the spiral tool path, which is widely used for turning freeform surfaces and Fresnel optics, is no longer feasible for freeform Fresnel optics. Thus, a new tool path strategy termed the quasi-spiral path is proposed where the tool follows a contour curve instead of a spiral path. Considering the complexity and asymmetry of freeform Fresnel optics, the control points and feed per rotation for tool path planning are determined adaptively.

(3) Following the quasi-spiral path, the rake face of the tool is no longer naturally aligned with the cutting direction, which will potentially cause severe tool interference. To avoid tool interference, in addition to the position of the tool, the orientation of the tool also requires manipulation, which is similar to the "pose control." Thus, a scheme called the adaptive tool pose manipulation is proposed to manipulate the rake face direction during the machining process. In the adaptive tool pose manipulation framework, when observed from the coordinate system of the workpiece, the tool rotates around a virtual axis that moves continuously along a calculated path while varying the instantaneous radius as well as automatically aligning the normal of the rake face with the cutting direction. In addition, the adaptive tool pose manipulation can be achieved with only four axes (X, Y, Z, C), commonly seen in commercial UPM machines. This method can be regarded as a generic form of cutting tool pose control (considering the orientation of the rake face in addition to position) with four degrees of freedom.

(4) The framework introduced above requires all four axes of the machine tool to move coordinately with no periodic patterns. This brings challenges to speed up the process while maintaining the acceleration of axes within the limitation. Thus, an optimization-based method is proposed to generate timestep history adaptively.

In this study, we propose a new scheme for ultra-precision machining of freeform Fresnel optics using only four axes (X, Y, Z, C), which is a viable solution with minimal motion axis requirements. This scheme is currently the only generic fabrication solution specifically for freeform Fresnel optics defined by multiple types of functions with different levels of complexity. We first provide a UPM-compatible geometry definition for freeform Fresnel optics, convert it to a novel quasi-spiral tool path, design an adaptive tool pose manipulation scheme to control the tool rake orientation during machining, and generate the timestep history with an optimization-based method. We also propose two tool compensation methods with different computational costs to further improve the accuracy of machined surface profiles. To verify the effectiveness of the introduced scheme, two freeform lenses and the corresponding tool trajectories are designed according to the proposed method. The examples introduced in this study only aim to demonstrate the feasibility of fabrication under different conditions, and the freeform Fresnel optics for a specific application require corresponding optical design. The machining accuracy of the resultant workpiece is verified with a white-light surface profilometer. The profiling error in the depth direction is within 0.1 μm. Finally, an optical system is constructed to demonstrate and verify the functionality of fabricated freeform Fresnel optics. The proposed new scheme also provides the theoretical foundation for ultra-precision machining of complex or discontinuous surfaces for broader applications in functional surfaces.

2. Methods

In the proposed scheme, there are four main steps to transform a freeform optics design to the tool trajectories for each axis (X, Y, Z, C) that machines the corresponding freeform Fresnel surfaces, as shown in Fig. 2(a).

Optics EXPRESS

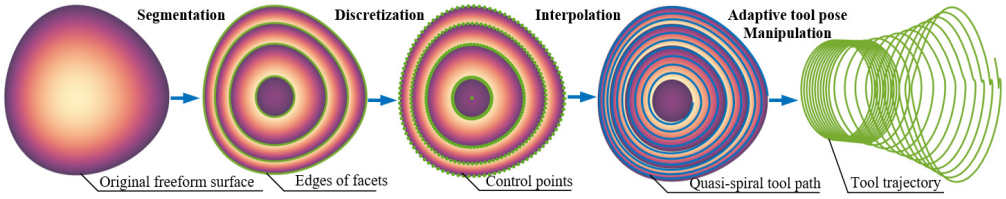

(a)

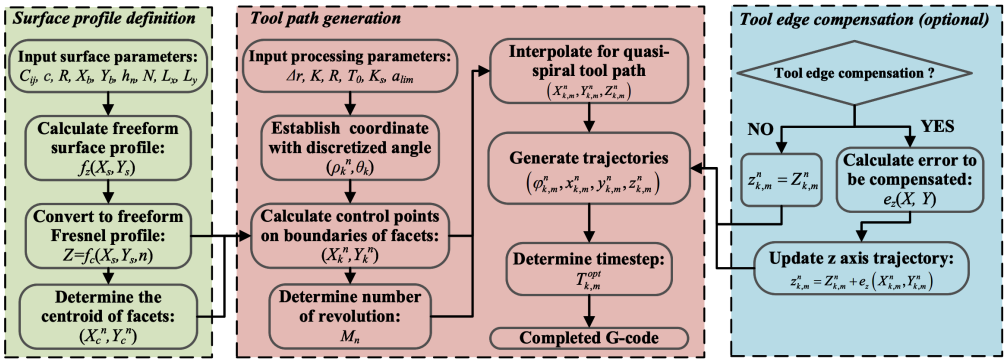

(b)

Fig. 2. (a) Basic steps from a given freeform surface profile to tool trajectories; (b) flowchart of the proposed scheme of freeform Fresnel optics fabrication.

Firstly, the original freeform profile is converted into a Fresnel form by slicing it along the contour line with a given thickness into multiple machinable facets. After the segmentation, the obtained profile of freeform Fresnel optics is discretized into sets of control points on the edges of facets. By filling the facets between edges with a continuous curve using linear interpolation, the control points on the edges are further interpolated to a quasi-spiral tool path. To follow the quasi-spiral tool path while aligning the normal tool rake face with the cutting direction, an adaptive tool pose manipulation framework is applied to map the quasi-spiral tool path in the workpiece coordinate to the trajectories of all four axes in the global coordinates. The detailed flow chart of the scheme is shown in Fig. 2(b), which is introduced from Section 2.1 to Section 2.5 in detail.

2.1. Profile generation of freeform Fresnel optics

In this study, freeform surfaces are defined in the coordinate system shown in Fig. 3(a), where a Cartesian coordinate X-O-Y is defined in the workpiece coordinate system with the origin fixed on the spindle axis, and X_s-O_s-Y_s is the freeform surface coordinate that defines the freeform surface. To facilitate the design of off-axis optics or lens arrays, the origin of the coordinate system where the freeform surface locates is not necessarily fixed on the spindle axis. As a result, the freeform surface is set to be defined at X_s-O_s-Y_s, which is offset by X_b and Y_b in the X and Y directions from the spindle axis Z, respectively.

The freeform surface is defined by a polynomial function in the freeform surface coordinate X_s-O_s-Y_s:

$$Z_s = f_z(X_s, Y_s) = \left(\frac{c\left(X_s^2 + Y_s^2\right)}{1 + \sqrt{1 - c^2\left(X_s^2 + Y_s^2\right)}} + \sum_i^I \sum_j^J C_{i,j} T_i\left(\frac{X_s}{L_x}\right) T_j\left(\frac{Y_s}{L_y}\right) \right), \quad (1)$$

Optics EXPRESS

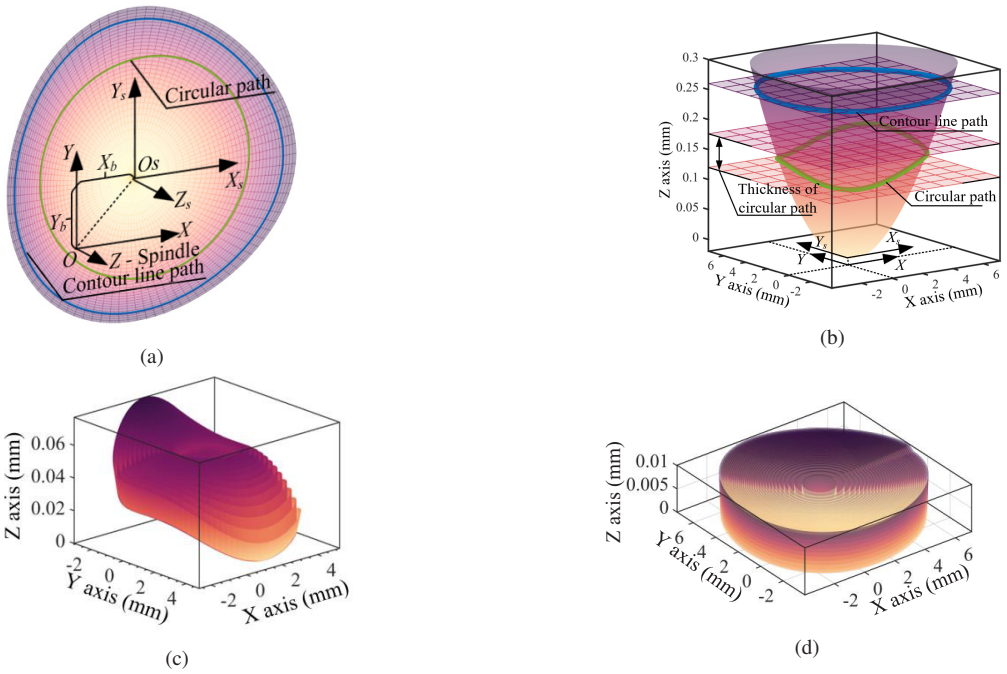

Fig. 3. (a) Coordinate definition for freeform optics; (b) 3-D drawing of example freeform optics; freeform Fresnel surfaces segmented by (c) circular paths and (d) contour paths.

where the first term is the spherical component that represents a basic spherical lens. T_i and T_j are the higher-order terms defined by Chebyshev polynomials [25]. In Eq. (1), c is the curvature of the spherical term, which represents the shape of a common spherical lens. And high order terms containing 2-D coefficient $C_{i,j}$ from the freeform surface within a reference region ($-L_x$, L_y to L_x, L_y). For Chebyshev polynomials, the ith higher order term $T_i(x)$ is given by:

$$T_i(x) = \cos(i \arccos(x)). \tag{2}$$

An example of a freeform surface using the definition in Eq. (1) is shown in Fig. 3(b), the parameters of which are listed in Table 1, Appendix A.1. (Parameters of two additional exemplary surfaces are listed in Table 2 and Table 3, respectively.) This is an off-axis freeform surface that lacks both rotational and axial symmetry and, therefore, does not conform to a specific design or shape. This complex surface, composed of a spherical term, two different 3rd order (no axial symmetry) freeform terms, and a biased origin, is used to verify the general feasibility of the proposed method on a non-specific freeform surface. To be noted, the Chebyshev polynomials can be replaced by other continuous and differentiable functions, such as Zernike or power polynomials, which can represent a freeform surface in a parametric form $Z = f_z(X_s, Y_s)$. The generality of the scheme is on its feasibility on different optical surfaces defined by different types of functions. Among variable surface profiles that Eq. (1) represents, the scheme introduced in this study is eligible for fabricating freeform surfaces with closed contour lines. The feasible extension of the proposed scheme in fabricating more complex freeform Fresnel surfaces is further discussed in Appendix A.2.

To convert a defined freeform surface into a Fresnel form, the segmentation path on the X-O-Y plane is required to slice a freeform surface into a set of facets. For Fresnel optics that reconstruct spherical and aspherical surfaces, slicing along circular (concentric) paths is commonly used, as shown by the green curve in Fig. 3(a). However, for many freeform optics designs, the depth in

Optics EXPRESS

the Z direction fluctuates along a circular path due to the lack of rotational symmetry. As a result, the height of facets segmented by a circular path fluctuates in the depth direction (Z-axis), as shown in Fig. 3(b). The use of a circular path to divide a freeform surface into facets for the purpose of constructing Fresnel optics has a major limitation. The thickness of the resulting Fresnel design is constrained by the fluctuations in depth along the circular path, regardless of the level of refinement applied to the segmentation process, as shown in Fig. 3(c). To address this challenge, the freeform surface is sliced (at a different height than the circular path in Fig. 3(b)) by a contour line path with a constant Z_s shown in the blue line of Fig. 3(a) and 3(b). By slicing the freeform surface along a single contour line path, which is perpendicular to its local gradient and maintains a constant coordinate on the Z-axis, it is possible to achieve a theoretically zero thickness in the design. This eliminates the fluctuations in the depth direction and overcomes the limitations encountered with circular paths.

Therefore, the freeform surface can be directly transferred to a Fresnel form composed of a set of facets by segmentation according to a constant depth increment. If the thickness of the nth facet (starting from outside to inside) is set to be h_n, the surface profile of the nth facet can be represented by the original surface profile with additional discrete terms calculated by h_1 to h_n:

$$f_c\left(X_s, Y_s, n\right) = \left(\frac{c\left({X_s}^2 + {Y_s}^2\right)}{1 + \sqrt{1 - c^2\left({X_s}^2 + {Y_s}^2\right)}} + \sum_i^I \sum_j^J C_{i,j} T_i\left(\frac{X_s}{L_x}\right) T_j\left(\frac{Y_s}{L_y}\right) \right) - Z_0 + \sum_{l=1}^{n} h_l, \quad (3)$$

where $Z_0 = \sum_{n=1}^{N} h_n$ is the total height of a sliced freeform surface and $\sum_1^n h_n$ is the total height of the first to the nth facets. Here, a constant thickness h_n is used to slice the freeform surface, the result of which is shown in Fig. 3(d). The thickness of the resultant freeform Fresnel surface is monotonously constrained by the density of segmentation, which can be theoretically refined to zero. The resulting surface profile is composed of facets with continuous, closed, and non-rotationally symmetrical contour lines, making it a machinable design, unlike previous designs from [1] that were represented by facet arrays and could not be machined.

2.2. Generation of quasi-spiral tool paths

To fabricate the freeform Fresnel optics obtained from the proposed segmentation strategy with UPM, a new tool path planning strategy termed quasi-spiral tool path is proposed. For the fabrication of Fresnel optics, the spiral tool path is commonly utilized, where an axis parallel to the surface of the workpiece (X-axis) feeds at a certain speed while the axis perpendicular to the surface of the workpiece (Z-axis) moves progressively. However, when using a spiral tool path in the diamond turning of freeform Fresnel optics, the tool will pass the edges of facets in a direction that deviates from the local tangential direction. As a result, severe flank interference will occur, as shown in Fig. 4(a). Therefore, similar to the above-mentioned segmentation methods, it is natural to follow a quasi-spiral tool path approximately along the contour line on each facet shown in Fig. 4(b) to machine the freeform Fresnel surface. Since the cutting direction is always approximately tangent to the edges of facets by using a quasi-spiral tool path, the undesired flank face interference in Fig. 4(a) is avoided.

A smoother transition between facets is achieved by using control points on the edges of the facets rather than generating the quasi-spiral tool path directly through gradient-based searching. This approach eliminates unwanted fluctuations in the Z-axis motion (depth direction) and reduces computational effort compared to the previous method. Since the freeform Fresnel surface in the workpiece coordinates (X, Y) is biased by X_b and Y_b, (X_s, Y_s) in the freeform surface coordinate can be represented by $X_s = X - X_b, Y_s = Y - Y_b$. Then, in the workpiece coordinate (X, Y), the edge of the nth facet can be represented by:

$$f_c\left(X - X_b, Y - Y_b, n\right) = h_n. \quad (4)$$

Optics EXPRESS

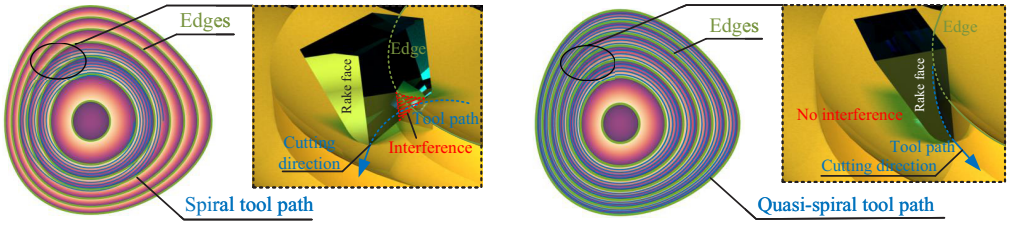

Fig. 4. (a) Conventional spiral tool path and resultant possible interference; (b) proposed quasi-spiral tool path.

The corresponding resultant edges of facets are shown in Fig. 5(a). To calculate control points on the nth edge of the facet, a polar coordinate is established at the centroid (X_c^n, Y_c^n) of the area within it, and the control points are assigned with equal angular increments:

$$\begin{cases} X_k^n = X_c^n + \rho_k^n cos\theta_k \\ Y_k^n = Y_c^n + \rho_k^n sin\theta_k \end{cases}, \tag{5}$$

where θ_k (k=1, 2, . . . , K) ranges from 0 to 2π; and (X_c^n, Y_c^n) is calculated by:

$$\begin{cases} X_c^n = \dfrac{\oint_{fc(X-X_b,Y-Y_b,n)\le h_n} XdXdY}{\oint_{fc(X-X_b,Y-Y_b,n)\le h_n} dXdY} \\ Y_c^n = \dfrac{\oint_{fc(X-X_b,Y-Y_b,n)\le h_n} YdXdY}{\oint_{fc(X-X_b,Y-Y_b,n)\le h_n} dXdY} \end{cases}. \tag{6}$$

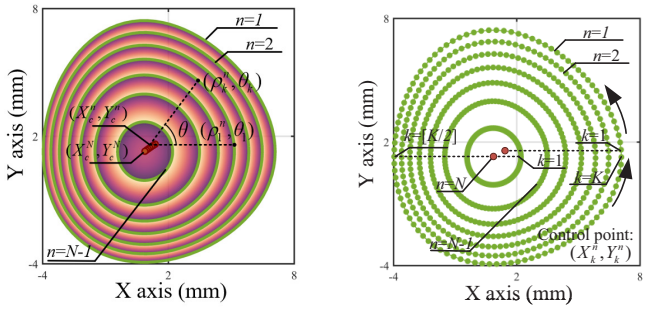

Fig. 5. (a) Determination of control points on edges of facets with polar coordinates located at the centroid; (b) obtained control points on the X-O-Y plane.

By substituting the given angular coordinate θ_k in Eq. (5) and the centroid (X_c^n, Y_c^n) obtained from Eq. (6) into Eq. (4), with the obtained ρ_k^n using the golden section search, the control points of the nth edge at the kth angle (X_k^n, Y_k^n) is obtained as shown in Fig. 5(b). To be noted, the control points shown in the figure are for illustration purposes and are significantly lower in density compared with the actual generated points.

This quasi-spiral tool path strategy is applicable to most freeform Fresnel optics with closed contour lines. However, there may be certain exceptions, such as contour lines in the shape of a "C" or "U", where the distribution of control points becomes uneven or where there are multiple solutions for ρ_k^n for a given θ_k. For these special circumstances, an alternative control points

Optics EXPRESS

selection strategy using gradient-based searching is provided. Please refer to Appendix A.3 for more detailed information.

To form the desired freeform Fresnel surface, the gaps between the control points on the edges of the facets are filled using a quasi-spiral tool path that is generated through rotation-by-rotation interpolation. In freeform Fresnel optics, the local straight-line distance between two adjacent edges of facets is constantly changing, which makes it difficult to maintain a constant feed per rotation. To overcome this challenge, the total number of rotations on each facet is adaptively determined, which is called M_n. The following equation is used to calculate the number of rotations required between two edges of facets in order to ensure that the actual feed per rotation does not exceed a specified value Δr throughout the quasi-spiral tool path:

$$M_n \approx \frac{h_n/\Delta r}{\min_{k=1,2,\ldots,k} \left\| \nabla f_z(X_k^n - X_b, Y_k^n - Y_b) \right\|} \tag{7}$$

Then, at the mth rotation ($1 \le m \le M_n$), the quasi-spiral tool path is linearly interpolated with the obtained control points, where the kth point in the mth rotation $(X_{k,m}^n, Y_{k,m}^n, Z_{k,m}^n)$ is represented by:

$$\begin{cases} X_{k,m}^n = \frac{m(k-1)}{M_n K}(X_k^{n+1} - X_k^n) + X_k^n \\ Y_{k,m}^n = \frac{m(k-1)}{M_n K}(Y_k^{n+1} - Y_k^n) + Y_k^n \\ Z_{k,m}^n = f_c\left(X_{k,m}^n - X_b, Y_{k,m}^n - Y_b, n\right) \end{cases} \tag{8}$$

In this design, the coordinates in the depth direction, $Z_{k,m}^n$, are determined using Eq. (3) instead of interpolating the control points located at the edges of the facets to ensure forming accuracy on each interpolated point. The resulting interpolated quasi-spiral tool path, which fills the space between two adjacent edges of facets on the X-O-Y plane, is illustrated in Fig. 6.

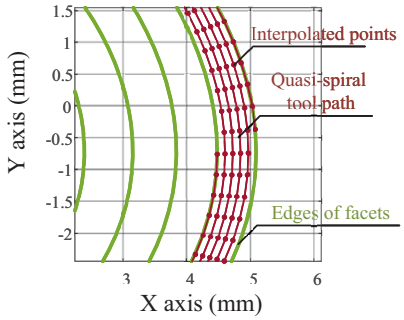

Fig. 6. Interpolated quasi-spiral tool paths between the two boundaries of facets.

2.3. *Adaptive tool pose manipulation*

To fabricate freeform Fresnel optics using the quasi-spiral tool path without encountering tool interference, a conventional (X, Z, C) configuration for the ultra-precision turning process is inadequate. To achieve the desired outcome, an additional Y axis must be incorporated into the turning process. The four-axis configuration (X, Y, Z, C) will allow real-time manipulation of the normal of the tool rake face.

With a conventional (X, Z, C) configuration, the X-axis is periodically moved during each rotation to match the cutting direction to follow the tangential direction of the local contour line. This allows for the cutting direction to stay aligned with the tool path. However, due to the rake face of the tool being perpendicular to the line connecting the origin O, rather than the

Optics EXPRESS

local gradient, the cutting direction will deviate from the normal of the rake face, resulting in an "oblique cutting process," as depicted in Fig. 7(a). As a consequence, flank interference occurs on the tool edge, as shown in Fig. 7(b). Also, as shown in the smaller contour in Fig. 7(a), if the quasi-spiral path is off-axis, sometimes the rake face will be opposite to the cutting direction, which is unacceptable for the turning process. In addition, the actual tool nose radius will change as the projection of the tool rake face in the cutting direction changes continuously in the "oblique cutting process," resulting in a non-uniform surface finish.

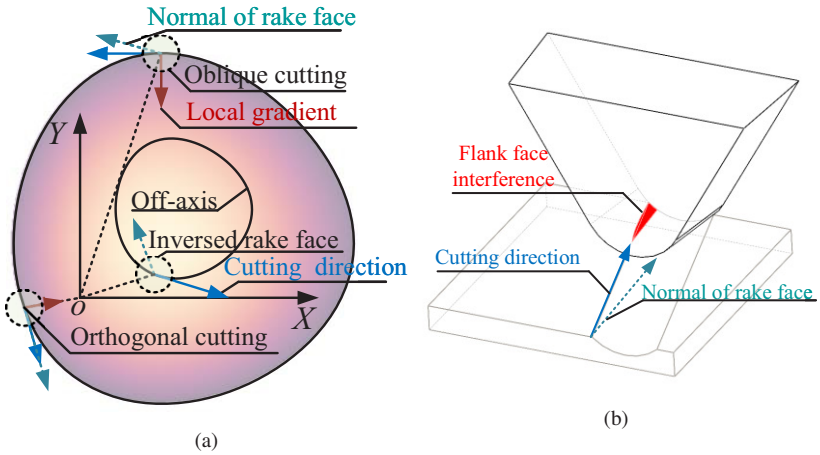

Fig. 7. (a) Schematic showing the oblique and orthogonal cutting paths; (b) illustration of interference in oblique cutting.

Thus, it is necessary to add an additional motion axis during the cutting process to adjust the normal direction of the rake face in real-time so as to coincide with the cutting direction. Then, the position and orientation of the cutting tool are collaboratively manipulated, similar to a "pose control." The (X, Y, Z, C) layout is a commonly used configuration for a 4-axis ultra-precision turning setup. In this context, an adaptive scheme for the 4-axis tool path planning is proposed as a solution for real-time manipulation of the rake face direction, which incorporates the motion of the Y-axis.

The proposed framework, illustrated in Fig. 8, involves rotating the workpiece around the C-axis while simultaneously rotating the workpiece coordinate X-O-Y clockwise by an angle φ around the Z-axis. The global coordinate x-o-y remains stationary while the cutting tool and machine tool move according to the coordinates x, y, z, and φ.

In the adaptive tool pose manipulation framework, all linear axes move accordingly as the spindle rotates to manipulate the normal of the rake face in real-time. The turning process during one rotation for machining freeform Fresnel optics is used as an example in Fig. 9(a) and 9(b), where the tool path in the workpiece coordinate is approximated as a closed contour line. Then, for each instance, the movement direction of the cutting point in the global coordinates is orientated to the rake face once even the rake face is erratically rotating in the workpiece coordinate $(X - O - Y)$. As a result, the cutting direction is always orthogonal to the local gradient of the quasi-spiral path, which heads to the center of the local osculating circle (dotted purple circle in Fig. 9) so as to maintain the orthogonal cutting condition during the entire rotation.

The adaptive tool pose manipulation framework provides an intuitive and comprehensive approach to coordinate all motion axes in turning freeform Fresnel surfaces. To generate the actual trajectory accordingly, the adaptive tool pose manipulation is transformed into two equivalent conditions. (1) The tool position (x, y) after rotating the angle φ is on the corresponding point of the quasi-spiral path (X, Y). (2) The normal of the tool rake face deviates from the cutting

Optics EXPRESS

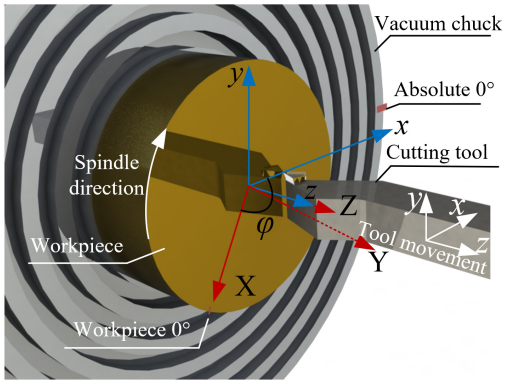

Fig. 8. Geometric definition of turning process.

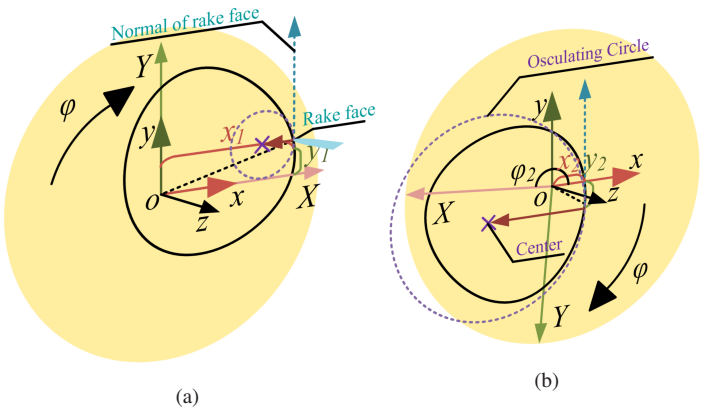

Fig. 9. Frames of a rotation of turning process with adaptive tool pose manipulation when (a) $\varphi = 0$, (b) $\varphi > 0$

direction (perpendicular to the local gradient) by an assigned history $\Delta\varphi$. By using these two conditions, for a given quasi-spiral tool path consisting of $(X^n_{k,m}, Y^n_{k,m})$, the φ, x, y components at the kth angle θ of the mth rotation on the nth facet $(\varphi^n_{k,m}, x^n_{k,m}, y^n_{k,m})$ can be collectively calculated by the following equation:

$$\begin{bmatrix} X^n_{k,m} \\ Y^n_{k,m} \\ \frac{\partial_X f_z(X-X_b,Y-Y_b)}{\|\nabla f_z(X-X_b,Y-Y_b)\|} \\ \frac{\partial_Y f_z(X-X_b,Y-Y_b)}{\|\nabla f_z(X-X_b,Y-Y_b)\|} \end{bmatrix} = \begin{bmatrix} \cos(\varphi^n_{k,m}) & \sin(\varphi^n_{k,m}) & 0 & 0 \\ -\sin(\varphi^n_{k,m}) & \cos(\varphi^n_{k,m}) & 0 & 0 \\ 0 & 0 & \cos(\varphi^n_{k,m}) & \sin(\varphi^n_{k,m}) \\ 0 & 0 & -\sin(\varphi^n_{k,m}) & \cos(\varphi^n_{k,m}) \end{bmatrix} \begin{bmatrix} x^n_{k,m} \\ y^n_{k,m} \\ -\cos\Delta\varphi \\ \sin\Delta\varphi \end{bmatrix} \tag{9}$$

Equation (9) shows that the 4-axis trajectory is gradient-related, which differentiates the proposed framework from the common tool path planning strategies that consider the position only. Besides the location of the tool, the rotary degree of freedom of the tool that governs the orientation of the tool face can be manipulated according to a desired history. For the fabrication of freeform Fresnel optics, the deviation between the cutting direction and the normal of the rake face $\Delta\varphi$ is assigned to 0 as illustrated in Fig. 9. Then the vector $[-\cos\Delta\varphi, \sin\Delta\varphi]$ in the last two rows of Eq. (9) is [-1, 0], indicating that the cutting direction is perpendicular to the tool rake face. $\Delta\varphi$ can be changed for a tailored rake face orientation history for other application

Optics EXPRESS

scenarios to avoid tool inference, such as optical features with large azimuthal slopes. It can also be seen from Eq. (9) that if the target random curve is second-order continuous, then the movement of each axis of the machine tool is first-order continuous, which can be programmed by a PVT (position-velocity-time) or PT (position-time) form.

Also, when turning along a circular contour line that forms an aspherical Fresnel lens, the last two rows that constrain the orientation of the rake face is automatically satisfied. As a result, by transferring the above two rows into a polar coordinate, the adaptive tool pose manipulation returns back to the virtual spindle scheme, which has been applied to machine lens arrays by [16]. Thus, the proposed adaptive tool pose manipulation scheme can be regarded as a complete and generic form of "cutting tool pose control" in the 4-axis machining configuration that covers the virtual spindle method in machining lens arrays. This framework can be applied to various scenarios where the turning of a complex contour is required. With the adaptive tool pose manipulation framework, the trajectories of X, Y, Z, C axes, as shown in Fig. 10(b), are obtained, which are represented by $\varphi^n_{k,m}$, $x^n_{k,m}$, $y^n_{k,m}$, $z^n_{k,m}$, respectively. In addition, the quasi-spiral path that shows the tool trajectory in the rotating workpiece coordinate is shown for comparison (when $\varphi = 0$, the workpiece coordinate and global coordinate coincide). Also, a lower density of facets and larger feed per rotation when compared to the actual process is applied to Fig. 10(b) to show the tool path without overlapping.

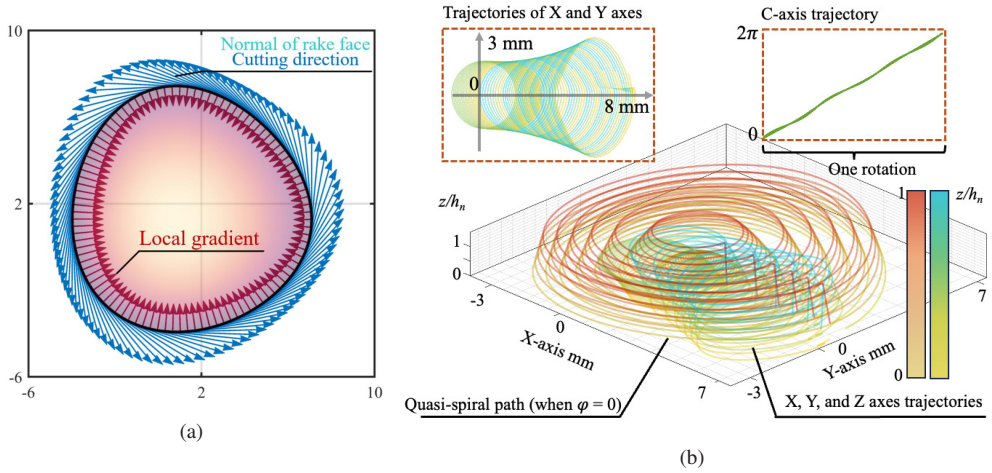

Fig. 10. (a) Real-time alignment of the normal of rake face and cutting direction in the workpiece coordinate; (b) quasi-spiral tool path and corresponding trajectories of C, X, Y, and Z axes while machining the exemplary freeform Fresnel surface.

2.4. *Tool edge compensation*

Unlike conventional freeform optics, the tool edge compensation for turning freeform Fresnel optics is achieved by offsetting the programming position on the z-axis based on the error between the actual cutting point on the tool edge and the theoretical programmed position, similar to the tool compensation used in Fresnel optics. As depicted in Fig. 11(a), the theoretical tool contact point is at point A, while there is an additional contact point of B at a distance $\Delta\rho$ from OA, which results in a local forming error of the machined profile. To compensate for this error, the tool moves a distance e_z in the $+z$-axis direction so that the tool edge has only one intersection point C with the desired profile. The value of e_z is the largest distance between the tool edge and the desired profile for all $\Delta\rho$. $\Delta\rho$ can be calculated by searching for the maximum distance in the

Optics EXPRESS

opposite direction of the local gradient:

$$e_z(X,Y) = \max_{\Delta\rho=[0,+\infty)} f_z\left(X_s + \frac{\partial_X f_z(X_s,Y_s)}{\|\nabla f_z(X_s,Y_s)\|}\Delta\rho, Y_s + \frac{\partial_Y f_z(X_s,Y_s)}{\|\nabla f_z(X_s,Y_s)\|}\Delta\rho\right) - f_z(X_s,Y_s) - \left(R - \sqrt{R^2-\Delta\rho^2}\right) \tag{10}$$

where $X_s = X - X_b, Y_s = X - Y_b$. In Eq. (10), the partial differential of f_z is calculated by:

$$\begin{cases} \frac{\partial f_z(X_s,Y_s)}{\partial X_s} = -\left(\frac{cX_s}{\sqrt{1-c^2\left({X_s}^2+{Y_s}^2\right)}} + \sum_{i=0}^{I}\sum_{j=0}^{J} C_{i,j}\frac{i\sin\left(i\cos^{-1}\left(\frac{X_s}{L_x}\right)\right)}{\sqrt{1-\frac{{X_s}^2}{L_x}}}\cos\left(j\cos^{-1}\left(\frac{Y_s}{L_y}\right)\right)\right) \\ \frac{\partial f_z(X_s,Y_s)}{\partial Y_s} = -\left(\frac{cY_s}{\sqrt{1-c^2\left({X_s}^2+{Y_s}^2\right)}} + \sum_{i=0}^{I}\sum_{j=0}^{J} C_{i,j}\cos\left(i\cos^{-1}\left(\frac{X_s}{L_x}\right)\right)\frac{j\sin\left(j\cos^{-1}\left(\frac{Y_s}{L_y}\right)\right)}{\sqrt{1-\frac{{Y_s}^2}{L_y}}}\right) \end{cases} \tag{11}$$

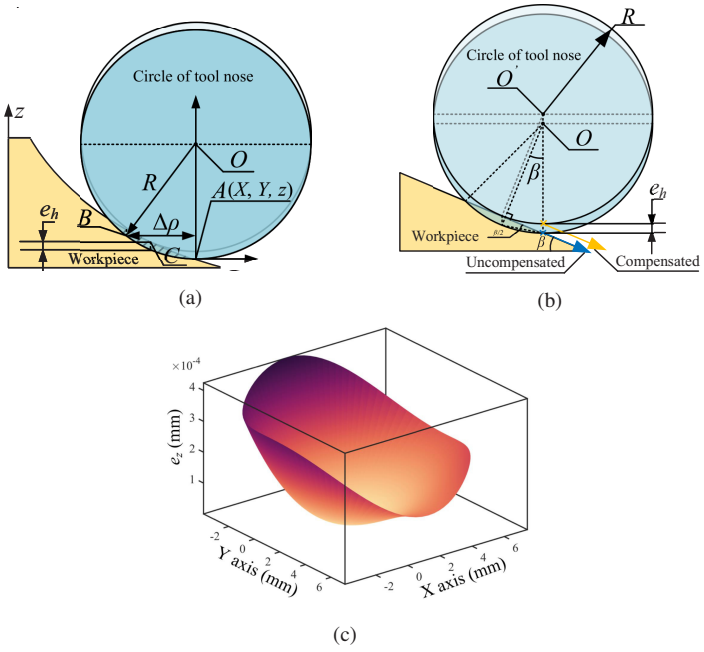

Fig. 11. (a) Tool edge compensation on freeform Fresnel optics; (b) simplified tool edge compensation on a straight line; (c) calculated distribution of tool edge compensation error e_z.

For the demonstrated example, the calculated distribution of e_z based on Eq. (10) for a 40 μm nose radius tool is shown in Fig. 11(c). The maximum e_z is calculated to be 400 nm. Thus, tool compensation is required for the optimal performance of the machined freeform Fresnel optics.

Additionally, because the slope variation along the local gradient direction is minimal near the cutting edge for many freeform Fresnel optical designs, the local surface profile can be approximated as a straight line, as illustrated in Fig. 11(b). To reduce computational effort, the compensation error e_z can be explicitly calculated given the geometric constraints:

$$\begin{cases} e_z(X,Y) = R\tan(\beta)tan(\beta/2) \\ \beta = \arctan\|\nabla f_z(X_s,Y_s)\| \end{cases} \tag{12}$$

Optics EXPRESS

For the given example, the maximum difference between e_z calculated by Eq. (10) and Eq. (12) is below 10 nm, which is an adequate estimation for the cutting edge compensation. Finally, the actual trajectory of the Z-axis $z^n_{k,m}$ is updated by adding the compensation error e_z to the original Z-axis coordinate of the quasi-spiral path:

$$z^n_{k,m} = Z^n_{k,m} + e_z(X^n_{k,m}, Y^n_{k,m}). \tag{13}$$

By combining the calculation results of $\varphi^n_{k,m}$, $x^n_{k,m}$, $y^n_{k,m}$, $z^n_{k,m}$ from Eq. (9) and Eq. (13) for all k, m, n in sequence, a complete tool path for cutting freeform Fresnel optics is obtained, which is further converted to position-time interpolated curves interpreted by the machine tool.

2.5. Adaptive determination of timesteps

The generated trajectories are transformed into G-code in a position-time format, with all available position channels (X, Y, Z, C) fully defined by $\varphi^n_{k,m}$, $x^n_{k,m}$, $y^n_{k,m}$, $z^n_{k,m}$. However, the timesteps can still be adjusted to optimize the acceleration of each axis and improve process efficiency. Nevertheless, even though the four axes work in tandem, accelerating one axis may lead to a trade-off with another. During a rotation, simply reducing the acceleration of one axis by changing the timestep under the same total time consumption could result in a significant increase in the acceleration of another axis because they share the same timestep while moving independently. Therefore, here, an optimization-based method to adaptively determine the timestep during the machining process is proposed to speed up the process while arranging the maximum acceleration of all axes within a safety zone.

During the cutting process, the acceleration of each axis can be calculated by a second-order difference. Take the X-axis for an example; the acceleration at the kth angle of the mth rotation $a^x_{k,m}$ can be written by:

$$a^x_{k,m} = 2\frac{\frac{x_{k+1,m}-x_{k,m}}{T_{k,m}} - \frac{x_{k,m}-x_{k-1,m}}{T_{k-1,m}}}{T_{k,m} + T_{k-1,m}} \tag{14}$$

Specifically, we set the initial and final values of the rotation angle $x_{k,m}$ to be the same as the final and initial values of the previous and next rotations, respectively. That is, $x_{k-1,m} = x_{K,m-1}$ when $k = 1$ and $x_{k+1,m} = x_{1,m+1}$ when $k = K$. By doing so, the generated trajectories form a smooth and continuous path without abrupt changes between adjacent rotations. For the reduction of the following error and stability of the machining process, the relative acceleration $a^x_{k,m}/a^x_{lim}$ should be kept below $1/K_s$. Thus, the optimization of the timesteps at all angles k of all rotations from 1 to M is required. However, since the whole process may contain millions of timesteps, the solution space is unacceptably large if a global optimization for all timesteps is performed. As the trajectories of several adjacent rotations are approximately periodic, the method of optimizing the acceleration of one rotation is used here to reduce the solution space, the formation of which is written as:

$$\begin{aligned} &\min_{T_{k,m}} \max_{k=1,\dots,K} \left| \frac{a^{\varphi}_{k,m}}{a^{\varphi}_{lim}}, \frac{a^x_{k,m}}{a^x_{lim}}, \frac{a^y_{k,m}}{a^y_{lim}}, \frac{a^z_{k,m}}{a^z_{lim}} \right| \\ &s.t. \sum_{k=1}^{K} T_{k,m} = KT_0 \end{aligned} \tag{15}$$

The cost function aims to minimize the maximum relative acceleration of all axes emerging during the mth rotation. The average of the timesteps is constrained to be equal to the reference timestep to prevent the solution from converging to extremely long timesteps, resulting in zero acceleration. The initial input of the first rotation is the reference timestep $T_{k,1} = T_0$. Then, the optimized solution of the mth rotation ($T_{1,m}$ to $T_{K,m}$) is used as the input of optimization of the $m + 1$th rotation to speed up the convergence. The optimization result of the first rotation of the exemplary freeform Fresnel optics is shown in Fig. 12(a) with the trajectories of the X- and Y-axes, respectively (for the exemplary freeform Fresnel optics, the relative acceleration is

Optics EXPRESS

mainly limited by the X- and Y-axes). The timestep increases while the velocity of the X, Y-axes changes dramatically and remains small when the movement of X, Y-axes is relatively steady. The acceleration calculated by the optimized timesteps is shown in Fig. 12(b). The maximum acceleration of each axis is reduced by around 50% within a rotation, resulting in a more uniform acceleration history during the machining process.

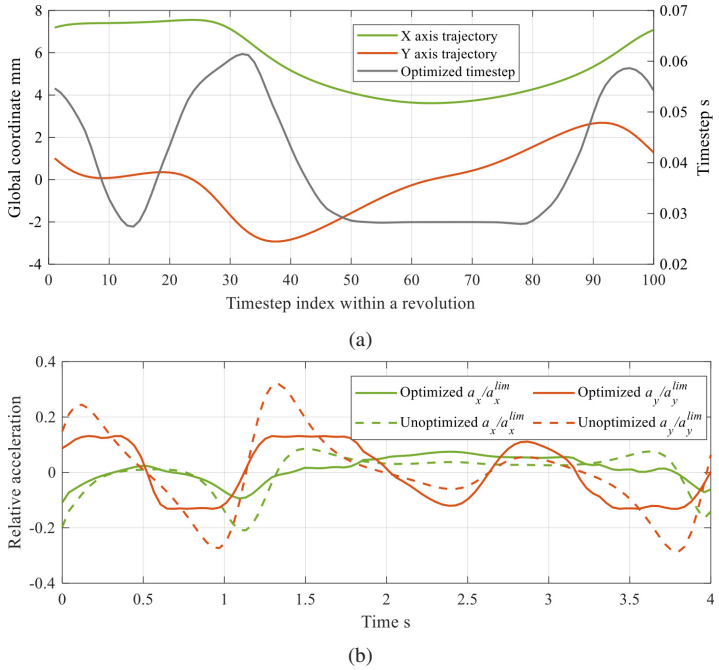

Fig. 12. (a) Trajectories of X, Y axes and optimized timestep in a rotation; (b) comparison of optimized and unoptimized acceleration of X, Y axes in a rotation.

With the optimized acceleration history, to speed up the machining process, the timesteps $T_{k,m}$ can be scaled down with the safety factor K_s by arranging the maximum relative acceleration occurred within the safety range:

$$T_{k,m}^{opt} = T_{k,m}\sqrt{K_s \max_{k=1,\ldots,K}\left|\frac{a_{k,m}^{\varphi}}{a_{lim}^{\varphi}}, \frac{a_{k,m}^{x}}{a_{lim}^{x}}, \frac{a_{k,m}^{y}}{a_{lim}^{y}}, \frac{a_{k,m}^{z}}{a_{lim}^{z}}\right|}. \tag{16}$$

The obtained final resultant timestep history $T_{k,m}^{opt}$ using the parameters listed in Table 4. Appendix A.1 is shown in Fig. 13. We observe that the spindle gradually speeds up as the average timestep of a rotation is decreasing while fluctuating. This is because a larger acceleration is required to move the axis over a longer range of motion, and as the range of motion decreases, a smaller acceleration is sufficient. The range of motion on each axis gets smaller rotation by rotation, resulting in a faster machining process. When the turning process comes near the center of the resultant freeform Fresnel optics, the contour lines become close to a point, and the timestep is approaching a constant value, indicating that the acceleration of the axes reaches a steady state. The process using the optimized timesteps takes 1 hour and 59 minutes, while the time consumption by simply using a constant timestep determined by the global maximum acceleration is 6 hours and 10 minutes. It should be noted that the improvement in production efficiency using the method depends on the geometry of the machined surface. For the exemplary design, the production efficiency is increased by more than three times.

Optics EXPRESS

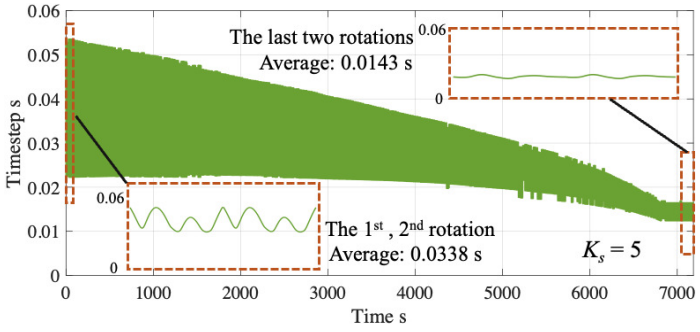

Fig. 13. Obtained timestep history from the initial to the final rotation of a complete machining process.

3. Experimental Verification

3.1. Experimental setup

To demonstrate the effectiveness of the proposed method, two freeform Fresnel optics designs were fabricated using ultra-precision diamond turning experiments. One of the designs is an off-axis freeform lens example, as discussed in Section 2. The other design is based on a provided freeform optic design based on Zemax proposed by [25] that involves the manipulation of irradiance. The videos of the ultra-precision turning process are included in the supplementary material. Both the accuracy of machined surface profiles and optical functions are evaluated in this section.

The experiments are conducted on an ultra-precision lathe (Nanoform X, Precitech, USA) with three linear axes (X, Y, Z) and a rotational axis (C), as shown in Fig. 14. A single-crystal diamond tool is adopted from Chardon Tool, USA, which has a 0° rake angle, 40 μm nose radius, and a 60° waviness window. To avoid interference when cutting the edges of facets, the diamond tool is designed with a split radius, the entering angle of which is designed to be 90° as shown in Fig. 14. The material of the workpieces used in this study is 360 brass.

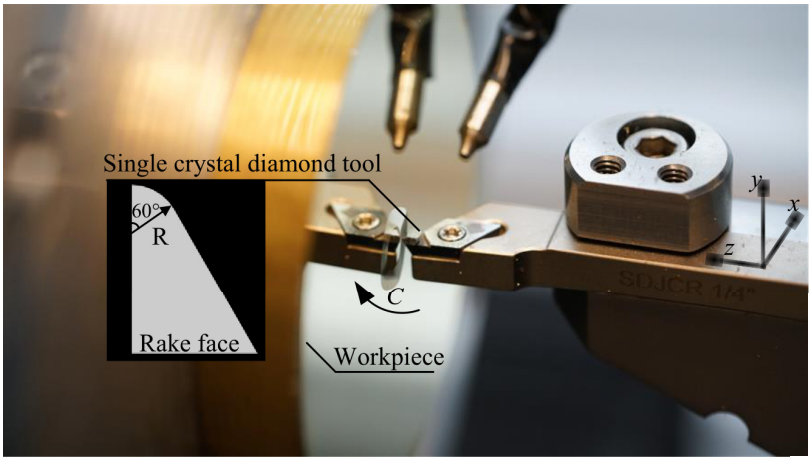

Fig. 14. Experimental setup and coordinate configuration (see experimental videos in Visualization 1 and Visualization 2).

Optics EXPRESS

3.2. Verification of the exemplary freeform Fresnel optics

The freeform Fresnel optic design introduced in Section 2 is successfully fabricated using UPM, and a stitched surface profile composed of 196 elementary images was obtained with a white light interferometer (NewView 7300, Zygo, USA). The resulting contour line, shown in Fig. 15(a), was compared with the desired contour line, and the forming error from 0 to 360° was calculated and displayed in Fig. 15(b). The maximum forming error was found to be within 10 μm over the 14 mm × 14 mm region, demonstrating high forming accuracy on the *X*-*O*-*Y* plane. Since the stitching of multiple images can cause cumulative errors in the depth direction, local comparisons were employed. To further verify the forming accuracy in the depth direction and assess the effectiveness of the tool compensation, a random region (0.352 mm × 0.264 mm) at the periphery of the optics was chosen. The desired profile, measured profile, and corresponding forming error of the resultant freeform Fresnel optic with compensation are displayed in Fig. 15(c) and 15(d), while those of the uncompensated ones are shown in Fig. 15(e) and 15(f). In Fig. 15(c) and 15(d), the desired and measured profiles exhibit excellent consistency, and the forming error is within ±100 nm, which is close to the specified forming accuracy of the lathe (100 nm). For the uncompensated profiles, the maximum forming error over the measured region reaches up to 791 nm, which is significantly larger than the compensated designs, revealing the effectiveness of the tool edge compensation. To validate the surface roughness, the surface microtopography of an arbitrary area of the machined surface is captured by a 3D laser confocal microscope (OLS5000, Olympus, USA), as shown in Fig. 15(g). An inclined line on the surface is chosen for measurement to avoid the edges of the facets, and the measured surface roughness provided by the laser confocal is 0.025 μm.

3.3. Verification of a freeform Fresnel optics transferred from Zemax example

To further verify the effectiveness of the proposed machining strategy to fabricate freeform Fresnel optics with deliberately tailored optical functions, an example of existing freeform optics design from the study of [25] is transferred to freeform Fresnel form, the parameters of which are shown in Table 2, Appendix A.1. The example here only aims to demonstrate the feasibility of fabrication, and the freeform Fresnel optics for a specific application require corresponding correction to compensate for the error brought up by segmentation. The geometry of the design is shown in Fig. 16(a), which aims to realize the function of irradiance manipulation that converts the original wavefront in Gaussian distribution to a square wavefront shown in Fig. 16(b).

The proposed method is applied to fabricate a freeform Fresnel optics with constant facet height h_n=10 μm, which is composed of 47 facets. The h_n is chosen to be 10 μm to demonstrate the ultra-thin feasibility while making the facets invisible by direct observation. Similar to Fig. 10(b), the generated quasi-spiral path and trajectories of all axes are shown in Fig. 16(c). The desired profile of the freeform optics is shown in Fig. 17(b), and the resulting freeform Fresnel optics on the workpiece surface is shown in Fig. 17(a) with a close-up view showing the facets. For this freeform Fresnel surface design, the process using the optimized timestep is measured to take 3 hours and 15 minutes, while the time consumption by using a constant timestep determined by the global maximum acceleration is 12 hours and 27 minutes. The grid on the background is distorted on the freeform Fresnel surface, revealing a "deceptive" concave area on the workpiece where the flat optics have only a thickness of 10 μm. To verify the forming accuracy of the freeform Fresnel optics, a quarter of the stitched surface profile from the measurement is attached to the desired profile for comparison. The contour lines of the measured profile, which correspond to the edges of the facets, are consistent with the desired profile, demonstrating the accuracy of the proposed method. To further evaluate the forming accuracy in the depth direction, a random region (0.352 mm × 0.264 mm) at the peripheral part of the optics is chosen for comparison without stitching error. The comparison of the desired profile and the measured profile is displayed in Fig. 17(c), while the error between them is shown

Optics EXPRESS

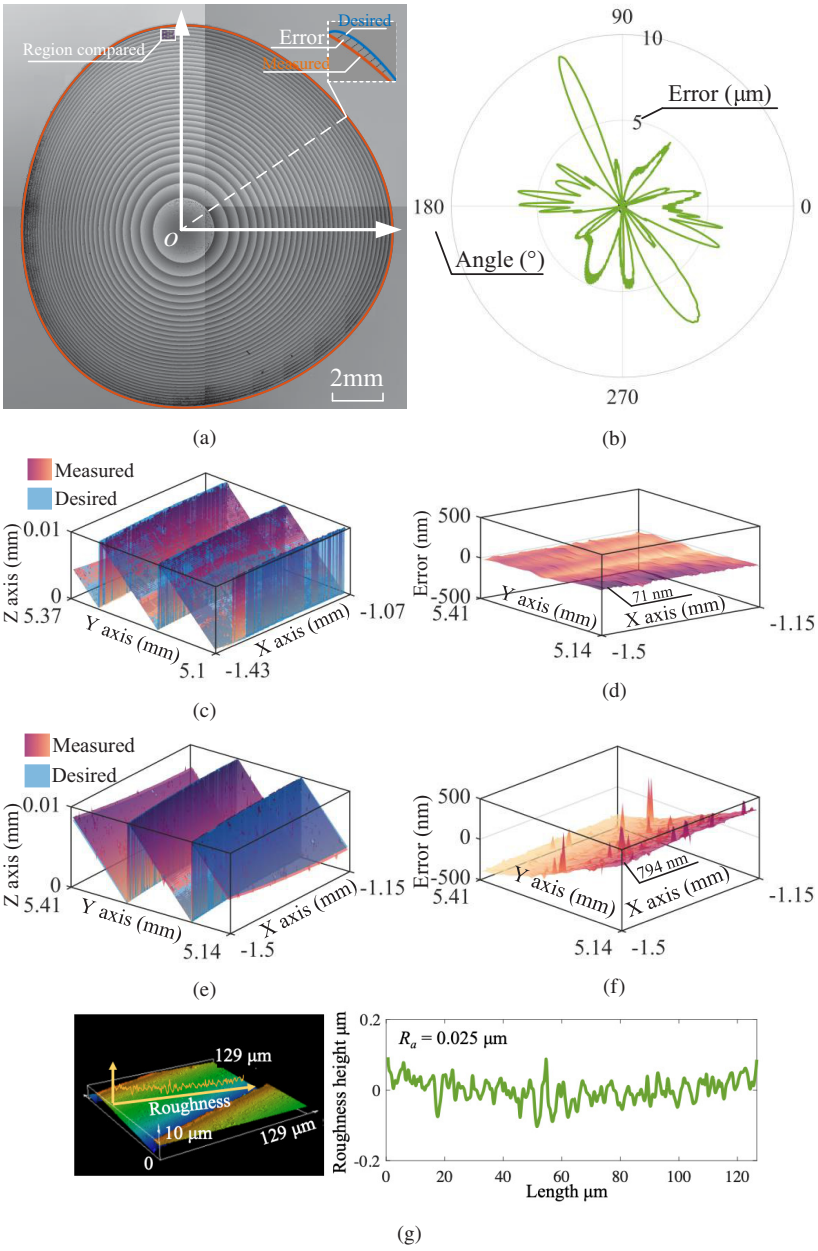

Fig. 15. (a) Stitched microscopic image of the resultant freeform Fresnel optics; (b) deviation of resultant contour line from desired profile; (c) comparison of the desired profile and measured profile of the freeform Fresnel optics processed with tool compensation and (d) corresponding forming error; (e) comparison of the desired profile and measured profile of the freeform Fresnel optics processed without tool compensation and (f) corresponding forming error; (g) measurement of surface roughness .

Optics EXPRESS

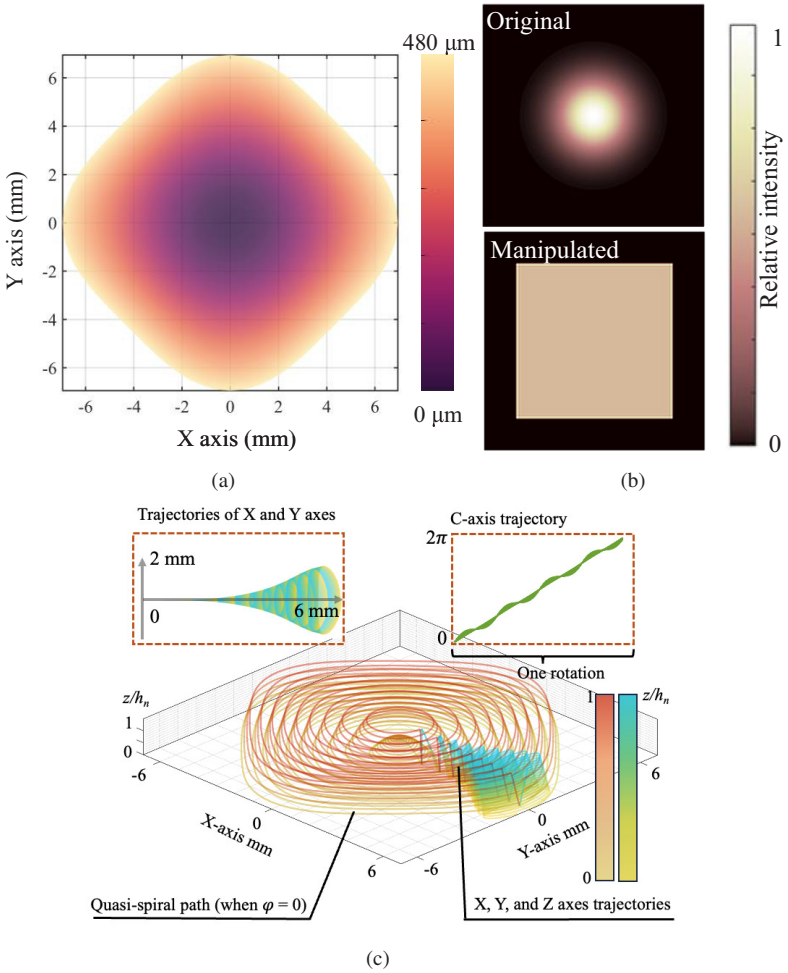

Fig. 16. (a) Depth map of the freeform optics design from Zemax; (b) original Gaussian wavefront, and manipulated square wavefront [25]; (c) quasi-spiral tool path and corresponding trajectories of C, X, Y, and Z axes while machining the freeform Fresnel surface.

in Fig. 17(d). The desired and measured profiles align excellently without visible deviation, and the forming error is within ±100 nm, which is close to the specified forming accuracy of the lathe (100 nm). Considering that an additional Y-axis is applied in the process, which may further influence the forming accuracy, the proposed method is demonstrated to be effective in achieving high forming accuracy. Additionally, as shown in Fig. 17(e), the surface roughness measured by the laser confocal is 0.016 μm.

In addition to verifying the surface profile, the optical function of the freeform Fresnel optics is also evaluated using a specially designed optical setup, as illustrated in Fig. 18(a). The setup involved directing the original wavefront from a 532 nm laser source onto a transflective lens, resulting in an image of the wavefront on a screen after reflection from a 45° mirror. A second

Optics EXPRESS

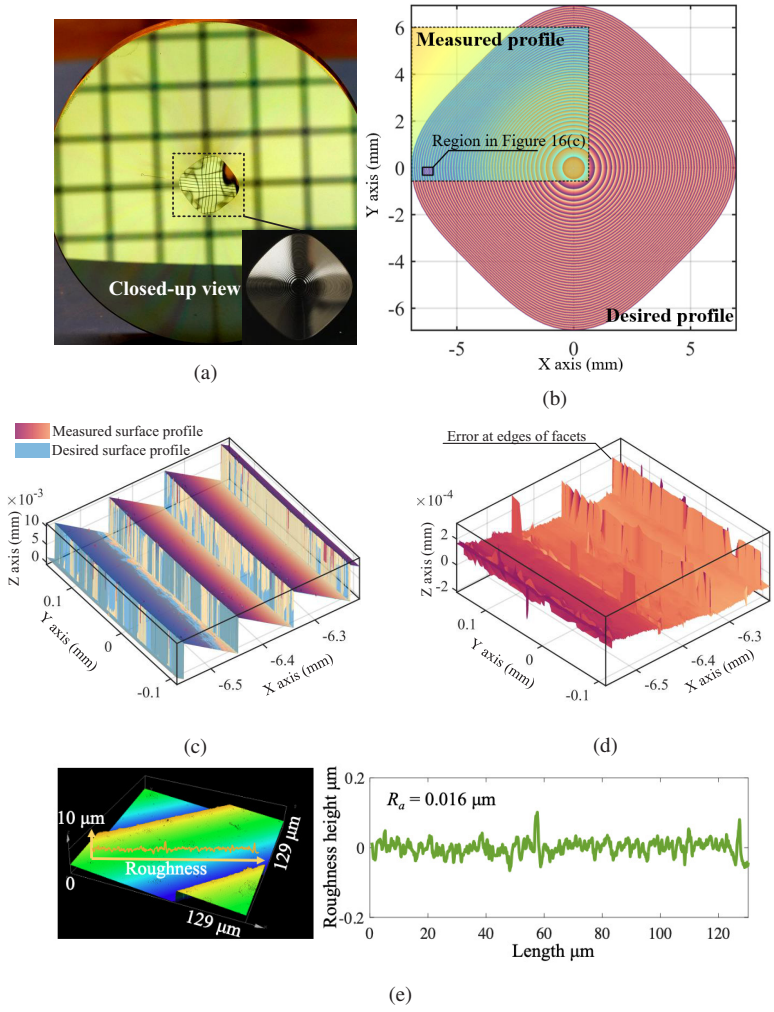

Fig. 17. (a) Picture of the resultant freeform Fresnel optics and the closed-up view; (b) comparison of the desired profile and measured profile of the freeform Fresnel optics on the *X-O-Y* plane; (c) comparison of the desired profile and measured profile of the freeform Fresnel optics on depth direction and (d) corresponding forming error; (e) measurement of surface roughness.

image of the manipulated wavefront was produced after reflection from the freeform Fresnel optics. A camera placed behind the screen captured simultaneous images of both wavefronts in the normal direction, as shown in Fig. 18(b). The original wavefront in Fig. 18(b) was transformed into a square wavefront as desired, consistent with the target optical functionality shown in Fig. 16(b). Therefore, the proposed method is capable of fabricating freeform Fresnel optics while maintaining the optical functionalities of the original optics.

Optics EXPRESS

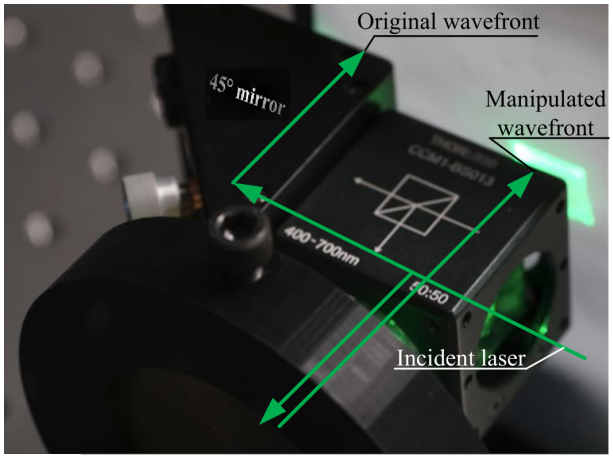

(a)

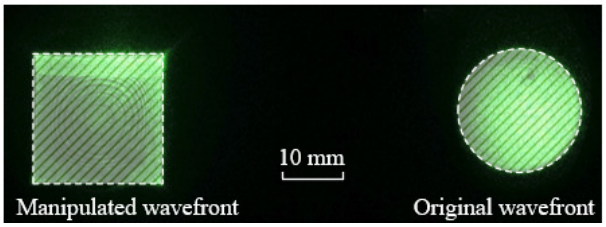

(b)

Fig. 18. (a) Picture of optical setup and laser; (b) original and manipulated wavefronts.

4. Conclusion

The fabrication of freeform Fresnel optics has been limited due to a lack of a scalable fabrication method. Existing industrial standard methods such as ultra-precision machining (UPM) face challenges, including tool interference induced by extreme asymmetry and discontinuity, as well as the absence of a unified geometry definition method. In this study, a scheme for fabricating freeform Fresnel optics using a minimal set of four axes (X, Y, Z, C) in ultra-precision turning is proposed. The scheme works as a generic fabrication solution for freeform Fresnel optics, as it is feasible for multiple types of geometry definitions.

The proposed method includes a geometry definition method that specifically addresses UPM, converting freeform surfaces to freeform Fresnel surfaces by slicing the surface along the contour lines. To overcome tool interference, a quasi-spiral tool path generation strategy is employed, which keeps the tool following the contour line of the machined facet. An adaptive tool pose manipulation method is also proposed to convert the quasi-spiral tool path to trajectories of axes while aligning the rake face of the tool with the cutting direction, further avoiding tool interference.

The study successfully fabricated two exemplary freeform optics with an ultra-precision lathe. The profiling error in the depth direction was found to be within 100 nm, and the optical function of a freeform Fresnel surface was verified by an optical setup. The main contributions of the study are fourfold:

(1) This work provides a complete routine for fabricating freeform Fresnel optics, including geometry definition, tool path planning, tool edge compensation, and timestep control, making it the first feasible approach for fabricating complex freeform Fresnel optics with UPM.

Optics EXPRESS

(2) The proposed adaptive tool pose manipulation method can be applied to the fabrication of different surfaces with complex geometries besides freeform optics. On the other hand, the framework can be regarded as a generic form of cutting tool pose control with 4 degrees of freedom by considering the manipulation of the orientation of the rake face. For example, high aperture lenses with a large slope can be machined without flank face interference by manipulating the orientation of the rake face in real-time.

(3) The proposed optimization-based method to adaptively determine the timestep history in tool path planning achieves the optimized machining efficiency while the acceleration of all axes is kept below the limit. This method can be applied to other multi-axis coordination with acceleration limitations.

(4) To address the technique gap of fabricating different freeform Fresnel optics, this work introduces adaptive solutions of tool path planning, manipulation of the pose of the cutting tool, and determination of timestep history, respectively. These computer-assisted manufacturing strategies are designed to be compatible with random geometries, which can be applied to the fabrication of various optics.

To improve the feasibility and production rate of the method, future work could focus on realizing a more adaptive compensation method. Additionally, extending the proposed method to surfaces with complex or discontinuous geometries presents a promising area for further investigation.

Nomenclature

(X_c^n, Y_c^n) The centroid of the area within the edge of the nth facet

$(X_k^n,\ Y_k^n)$ Control points of the nth edge at the kth angle

$(X_{k,m}^n,\ Y_{k,m}^n,\ Z_{k,m}^n)$ Quasi-spiral tool path at the kth point in the mth rotation and the nth facet

β Slope angle in the local gradient direction

$\Delta\varphi$ Deviation between the cutting direction and the normal of the rake face

$\Delta\rho$ Horizontal distance between the actual cutting point and the programmed point

$X,\ Y,\ Z$ Workpiece coordinates

φ Spindle angular position

$\varphi_{k,m}^n, x_{k,m}^n, y_{k,m}^n, z_{k,m}^n$ Trajectories of the C, X, Y, Z axes in the global coordinate

$a_{k,m}^{\varphi},\ a_{k,m}^{x},\ a_{k,m}^{y}$ Calculated accelerations of each axis at the kth angle during the mth rotation

$a_{lim}^{\varphi},\ a_{lim}^{x},\ a_{lim}^{y},\ a_{lim}^{z}$ Limitation of axis accelerations

c Curvature of the spherical term of freeform lens surface

C_{ij} Coefficient for the i,jth higher order terms of Chebyshev polynomials

h_n The height of the nth facet

$I,\ J$ Maximum order of the higher order terms

$i,\ j$ Indices for the higher order terms

$k,\ K$ Index and maximum number of discretized θ

K_s Safety coefficient for acceleration

Optics EXPRESS

L_x, L_y Reference length of Chebyshev polynomials

m, M_n Index and total number of rotations on the nth facet

n, N Index and total number of facets

R Nose radius of the diamond tool

$T^{opt}_{k,m}$ Resultant optimized timestep history

T_0 Reference timestep

T_i The ith order term of the freeform lens surface

$T_{k,m}$ Unscaled timestep used at the kth angle in the mth rotation

x, y, z Global coordinates

ρ, θ Workpiece polar coordinates

X_b, Y_b Bias of freeform surface definition in the workpiece coordinate along the X, Y axes

X_s, Y_s Freeform lens surface coordinates

$Z = f_c(X_s, Y_s, n)$ Parametric surface function for a freeform Fresnel lens surface

$Z = f_z(X_s, Y_s)$ Parametric surface function describing a freeform lens surface

Z_0 Reference depth

Appendix

A.1 Parameters of introduced freeform Fresnel optics

Parameters used for the fabrication of freeform Fresnel optics in the article is listed in the following tables, where unlisted parameters are set to the default value of zero.

Table 1. Parameters of exemplary freeform Fresnel optics.

Geometry parameters			
L_x	L_y	$C(4,1)$	$C(1,4)$
8 mm	8 mm	0.0010	0.0006
X_b	Y_b	c	Z_0
2 mm	2 mm	$-3e^{-4}mm^{-1}$	0.3 mm

Processing parameters			
K	Δr	R	h_n
100	2 µm	42.1 µm	10 µm

Optics EXPRESS

Table 2. Parameters of freeform Fresnel optics in Section 3.3.

Geometry parameters			
L_x	L_y	$C(0,0)$	$C(1,2)$
8 mm	8 mm	-0.0102	-0.00439
$C(2,1)$	$C(1,4)$	$C(4,1)$	$C(1,6)$
-0.00439	4.903e-4	4.903e-4	-1.603e-4
$C(6,1)$	$C(1,8)$	$C(8,1)$	$C(1,10)$
-1.603e-4	5.638e-5	5.638e-5	2.357e-5
$C(10,1)$	$C(1,12)$	$C(12,1)$	$C(1,14)$
2.357e-5	6.985e-6	6.985e-6	-3.423e-6
$C(14,1)$	Z_0		
-3.423e-6	0.48 mm		

Processing parameters			
K	Δr	R	h_n
100	2 μm	42.1 μm	10 μm

Table 3. Parameters of freeform Fresnel optics in Appendix A.3.

Geometry parameters			
C_1	C_2	C_3	C_4
0.2 mm	1	1	$\pi/3$
Z_0			
0.2 mm			

Processing parameters			
K	Δr	R	h_n
200	5 μm	107 μm	10 μm

Table 4. Parameters used for the adaptive determination of the process timestep.

a^x_{lim}	a^y_{lim}	a^z_{lim}	a^{φ}_{lim}	K_s
500 mm/s^2	500 mm/s^2	500 mm/s^2	20 rad/s^2	5

A.2 Extension to the fabrication of more complex freeform surfaces

The proposed method for fabricating freeform Fresnel optics has some limitations. Specifically, it can only be used for surfaces with a single local minimum/maximum point and closed, continuous, and differentiable contour lines. To overcome this limitation, strategies need to be developed to extend the feasibility of the method for different surfaces. One possible approach could be to divide the freeform surface into several subregions and use supplementary curves. However, the methods for such extensions may vary depending on the surface being machined.

To illustrate this point, let us consider two examples. In the first example shown in Fig. 19(a), the freeform surface has two minimum points, making it impossible to process the resultant freeform Fresnel optics within a single turning process without tool retraction. To overcome this obstacle, the surface can be processed with three subregions separately, as shown in Fig. 19(b). By smoothing undifferentiable parts during control point selection, all subregions can be processed using the proposed scheme separately.

Optics EXPRESS

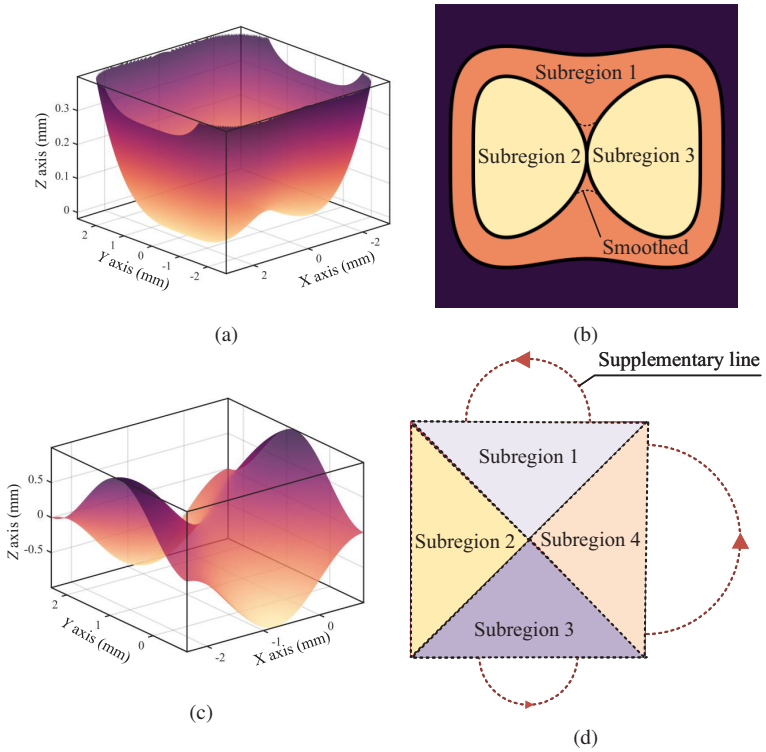

Fig. A1. (a) A freeform surface with multiple maximum and minimum points; and (b) the partition to subregions; (c) a freeform surface without closed contour lines and (d) the corresponding partition with supplementary paths.

In the second example, consider freeform surfaces without closed contour lines, such as Zernike's freeform surfaces shown in Fig. 19(c). In this case, generating a turning tool path along the contour lines is impossible. To address this challenge, supplementary lines are required to connect the starting and ending points of the contour line, as shown in Fig. 19(d). The supplementary line can be created by adding control points to an undefined region and forming a "close" contour line that constructs the quasi-spiral tool path.

A.3 An alternative scheme for generating control points

For some freeform surfaces, especially the freeform surfaces not included in the polynomial form represented by Eq. (1), the proposed method above to extract the control points of the freeform Fresnel optics is not applicable because of the emergence of uneven distribution and multiple solutions. Thus, an alternative scheme of control points determination based on searching along the tangential direction is provided here. For example, if the freeform surface is given by (Parameters are listed in Table 3):

$$z = f_z(X, Y) = C_1 \left(C_2 + C_3 \sqrt{X^2 + Y^2} \cos\left(\arctan\left(\frac{Y}{X} \right) + C_4 \right) \right), \tag{17}$$

the 3D profile of which is shown in Fig. 20(a). Then the total length of the edge of the nth facet is calculated by:

$$l_n = \oint_{f_z(X,Y) - Z_0 + \sum_{l=1}^{n} h_l = 0} \sqrt{dX^2 + dY^2}. \tag{18}$$

Optics EXPRESS

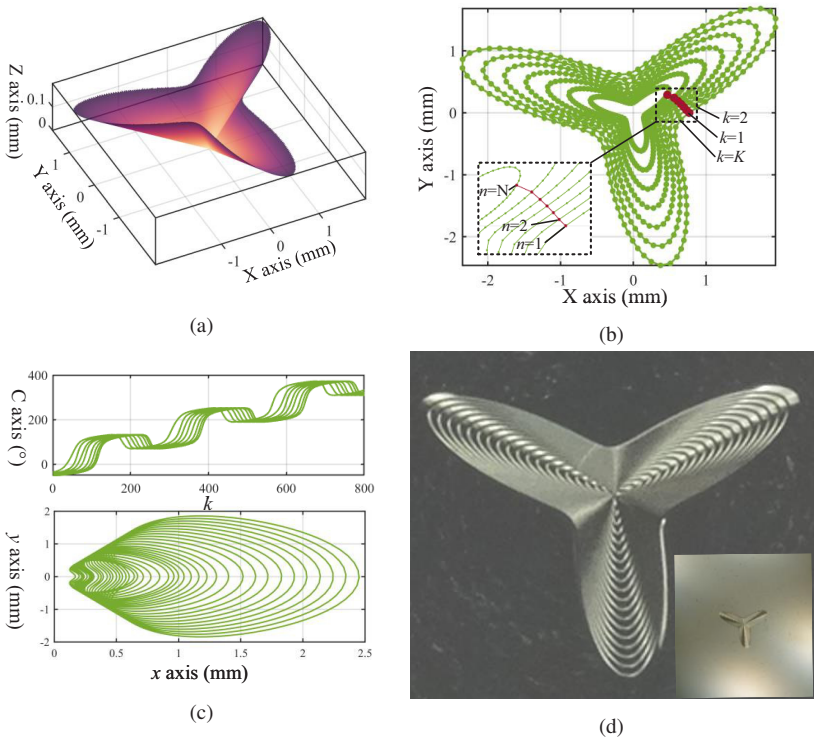

Fig. A2. (a) Exemplary freeform surface for alternative control points generation scheme; (b) control points generated by an alternative method in A.3; (c) corresponding generated tool path for the spindle and X, Y axes and (d) resultant machined surfaces.

If K points are selected on the edge of the nth facet, the length of the segment between each control point is l_n/K. Starting from a randomly selected initial point on the first edge ($n = 1, k = 1$), the initial point on the next edge is determined by searching along the local gradient direction, as shown in Fig. 20(b). Then, on the nth facet, with the kth obtained control point ($1 \leq k \leq K-1$) on $(X_k^n,\ Y_k^n)$, to find the $k+1$th control point, the point $(X_{k+1}^n,\ Y_{k+1}^n)$ that travels the certain distance along the tangential direction from $(X_k^n,\ Y_k^n)$ is searched by:

$$\int_{X_k^n, Y_k^n}^{X_{k+1}^n, Y_{k+1}^n} \sqrt{dX^2 + dY^2} - \frac{l_n}{K} = 0. \tag{19}$$

Then, on each facet, with the selected first points, all the control points from 1 to K can be obtained in sequence. By using the proposed method, control points that are evenly distributed along the boundaries can be obtained, regardless of the complexity of the contour lines, as demonstrated in Fig. 20(a). Once the control points are determined, the trajectories of the X, Y, C axes can be generated using the same procedure of interpolation and adaptive tool pose manipulation as described previously. The trajectories of the X, Y, C axes generated by the proposed method are shown in Fig. 20(c), while the corresponding cutting result is illustrated in Fig. 20(d).

Funding. National Science Foundation (CNS-2229170).

Disclosures. The authors declare no conflict of interest.

Data availability. Data underlying the results presented in this paper are not publicly available at this time but may be obtained from the authors upon reasonable request.

Optics EXPRESS

References

1. P. I. Goldstein, "Process for designing a freeform fresnel lens," Opt. Eng. **50**(12), 121703 (2011).
2. R. Kirrbach, M. Faulwaßer, and B. Jakob, "Non-rotationally symmetric freeform fresnel-lenses for arbitrary shaped li-fi communication channels," in *2019 Global LIFI Congress (GLC)*, (IEEE, 2019), pp. 1–6.
3. X. Hui, J. Liu, Y. Wan, *et al.*, "Realization of uniform and collimated light distribution in a single freeform-fresnel double surface led lens," Appl. Opt. **56**(15), 4561–4565 (2017).
4. D. K. Nikolov, A. Bauer, F. Cheng, *et al.*, "Metaform optics: Bridging nanophotonics and freeform optics," Sci. Adv. **7**(18), eabe5112 (2021).
5. N. Y. J. Tan, X. Zhang, D. W. K. Neo, *et al.*, "A review of recent advances in fabrication of optical fresnel lenses," J. Manuf. Process. **71**, 113–133 (2021).
6. J. P. Rolland, M. A. Davies, T. J. Suleski, *et al.*, "Freeform optics for imaging," Optica **8**(2), 161–176 (2021).
7. C.-T. Yen and S.-C. Jin, "Freeform surface lens design using genetic algorithm with acrylic material for reducing aberrations in multifocal artificial intraocular lens to enhance image sensing quality," Sens. Mater. **34**(1), 187–201 (2022).
8. A. Bruneton, A. Bäuerle, R. Wester, *et al.*, "High resolution irradiance tailoring using multiple freeform surfaces," Opt. Express **21**(9), 10563–10571 (2013).
9. X. Wang, Y. Qin, H. Hua, *et al.*, "Digitally switchable multi-focal lens using freeform optics," Opt. Express **26**(8), 11007–11017 (2018).
10. F. Fang, X. Zhang, A. Weckenmann, *et al.*, "Manufacturing and measurement of freeform optics," CIRP Ann. **62**(2), 823–846 (2013).
11. T. Fujita, H. Nishihara, and J. Koyama, "Blazed gratings and fresnel lenses fabricated by electron-beam lithography," Opt. Lett. **7**(12), 578–580 (1982).
12. B. Morgan, C. M. Waits, J. Krizmanic, *et al.*, "Development of a deep silicon phase fresnel lens using gray-scale lithography and deep reactive ion etching," J. Microelectromech. Syst. **13**(1), 113–120 (2004).
13. T. Aderneuer, O. Fernández, and R. Ferrini, "Two-photon grayscale lithography for free-form micro-optical arrays," Opt. Express **29**(24), 39511–39520 (2021).
14. I.-B. Sohn, M. S. Ahsan, Y.-C. Noh, *et al.*, "Fabrication of fresnel zone plate lens in fused silica glass using femtosecond laser lithography technology," Opt. Eng. **53**(5), 055107 (2014).
15. G. Shao, R. Hai, and C. Sun, "3d printing customized optical lens in minutes," Adv. Opt. Mater. **8**(4), 1901646 (2020).
16. W.-L. Zhu, F. Duan, X. Zhang, *et al.*, "A new diamond machining approach for extendable fabrication of micro-freeform lens array," Int. J. Mach. Tools Manuf. **124**, 134–148 (2018).
17. K. Nagayama and J. Yan, "Deterministic error compensation for slow tool servo-driven diamond turning of freeform surface with nanometric form accuracy," Journal of Manufacturing Processes **64**, 45–57 (2021).
18. H.-S. Kim, K.-I. Lee, K.-M. Lee, *et al.*, "Fabrication of free-form surfaces using a long-stroke fast tool servo and corrective figuring with on-machine measurement," Int. J. Mach. Tools Manuf. **49**(12-13), 991–997 (2009).
19. L. Zhu, Z. Li, F. Fang, *et al.*, "Review on fast tool servo machining of optical freeform surfaces," Int. J. Adv. Manuf. Technol. **95**(5-8), 2071–2092 (2018).
20. Y. Takeuchi, S. Maeda, T. Kawai, *et al.*, "Manufacture of multiple-focus micro fresnel lenses by means of nonrotational diamond grooving," CIRP Ann. **51**(1), 343–346 (2002).
21. R. Huang, X. Zhang, M. Rahman, *et al.*, "Ultra-precision machining of radial fresnel lens on roller moulds," CIRP Ann. **64**(1), 121–124 (2015).
22. D. W. K. Neo, A. S. Kumar, and M. Rahman, "An automated guilloche machining technique for the fabrication of polygonal fresnel lens array," Precis. Eng. **41**, 55–62 (2015).
23. L. Zhang, Y. Y. Allen, and J. Yan, "Flexible fabrication of fresnel micro-lens array by off-spindle-axis diamond turning and precision glass molding," Precis. Eng. **74**, 186–194 (2022).
24. K. Desnijder, P. Hanselaer, and Y. Meuret, "Freeform fresnel lenses with a low number of discontinuities for tailored illumination applications," Opt. Express **28**(17), 24489–24500 (2020).
25. B. Goodwin, U. Fuchs, S. Gangadhara, *et al.*, "Design and implementation of a new freeform surface based on chebyshev polynomials," in *Imaging and Applied Optics 2015*, (Optica Publishing Group, 2015), p. FT2B.3.